nature geoscience

Article

https://doi.org/10.1038/s41561-024-01555-6

Observed decrease in Deep Western Boundary Current transport in subpolar North Atlantic

Received: 3 August 2023

Accepted: 4 September 2024

Published online: 04 October 2024

Check for updates

G. Koman[1,2] ✉, A. S. Bower[1], N. P. Holliday[3], H. H. Furey[1], Y. Fu[4] & T. C. Biló[5,6]

The lower limb of the Atlantic Meridional Overturning Circulation is an important feature of Earth's climate system as it returns recently ventilated water to the deep ocean and is a major sink for anthropogenic carbon. The Deep Western Boundary Current—the primary component of the lower limb—flows southwards along the eastern flank of Greenland transporting dense water formed in the Nordic seas. Since 2014, the Deep Western Boundary Current has been continuously monitored at this location from a mooring array to observe the current's velocity and hydrographic structure close to its source. Here we find that the Deep Western Boundary Current transport has decreased by 26% over the first six years of observations, due to (1) a thinning of the traditionally defined Deep Western Boundary Current layer ($\sigma_\theta > 27.8$ kg m^{-3}) from a known freshening signal propagating through the subpolar region (56%), and (2) weakening velocities (44%). Despite this decrease, the Atlantic Meridional Overturning Circulation has remained relatively steady over the same period. Ultimately, this difference is due to the methods used to define these two circulations. Finding such notably different trends for two seemingly dependent circulations raises the question of how to best define these transports.

The Atlantic Meridional Overturning Circulation (AMOC) is an important component of Earth's climate system where warm water from the North Atlantic Current cools and subducts at high latitudes before returning southwards at depth (for example, ref. 1). The primary conduit of this return flow is the Deep Western Boundary Current (DWBC), although other interior pathways also exist (for example, refs. 2–6). Formed from Norwegian Sea overflow water entering the subpolar North Atlantic primarily through the Denmark Strait and the Faroe Bank Channel, the DWBC flows along the eastern flank of Greenland[7–12]. It is here that the Overturning in the Subpolar North Atlantic Program (OSNAP[13–15]) has monitored the DWBC since 2014 (Fig. 1). With moorings located near the southern tip of Greenland at Cape Farewell, OSNAP provides the longest continuous record of the DWBC in the Irminger Basin so far.

The first transport estimate of the DWBC (traditionally defined as flow of water with $\sigma_\theta > 27.8$ kg m^{-3} (refs. 10,16)) near Cape Farewell from continuous observations for more than 2 months found a transport of 9.0 Sv from instruments that were deployed from September 2005 to August 2006[17]. Synoptic realizations from hydrographic sections in the area have found DWBC transports ranging between 5.5 and 13.3 Sv (refs. 8,10,16,18–24). The best direct comparison with our study comes from Hopkins et al.[25], who assessed the OSNAP data from

[1]Woods Hole Oceanographic Institution, Woods Hole, MA, USA. [2]University of Massachusetts Boston, Boston, MA, USA. [3]National Oceanography Centre, Southampton, UK. [4]School of Earth and Atmospheric Sciences, Georgia Institute of Technology, Atlanta, GA, USA. [5]Cooperative Institute for Marine and Atmospheric Studies, University of Miami, Miami, FL, USA. [6]Atlantic Oceanographic and Meteorological Laboratory, National Oceanic and Atmospheric Administration, Miami, FL, USA. ✉e-mail: gregory.koman@umb.edu

https://doi.org/10.1038/s41561-024-01555-6

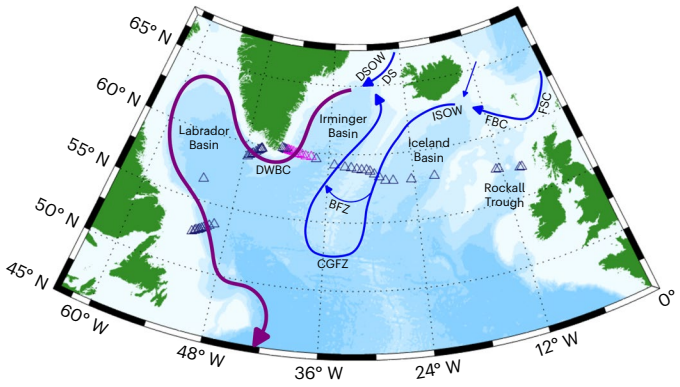

Fig. 1 | Deep water pathways in the North Atlantic subpolar region. Schematic of the deep water pathways in the North Atlantic subpolar region, adapted from Koman et al.[43]. The blue arrows indicate the pathways of the two primary water masses of Norwegian Sea Water origin (ISOW and DSOW), and the purple pathway depicts the DWBC (after the two water masses merge). All mooring locations in the OSNAP programme are denoted by triangles, with the moorings used in this study to determine the DWBC in magenta. Bathymetry colours change with every 1,000 m in depth. DS, Denmark Strait; ISOW, Iceland Scotland overflow water; FBC, Faroe Bank Channel; FSC, Faroe Shetland Channel; BFZ, Bight Fracture Zone; CGFZ, Charlie Gibbs Fracture Zone.

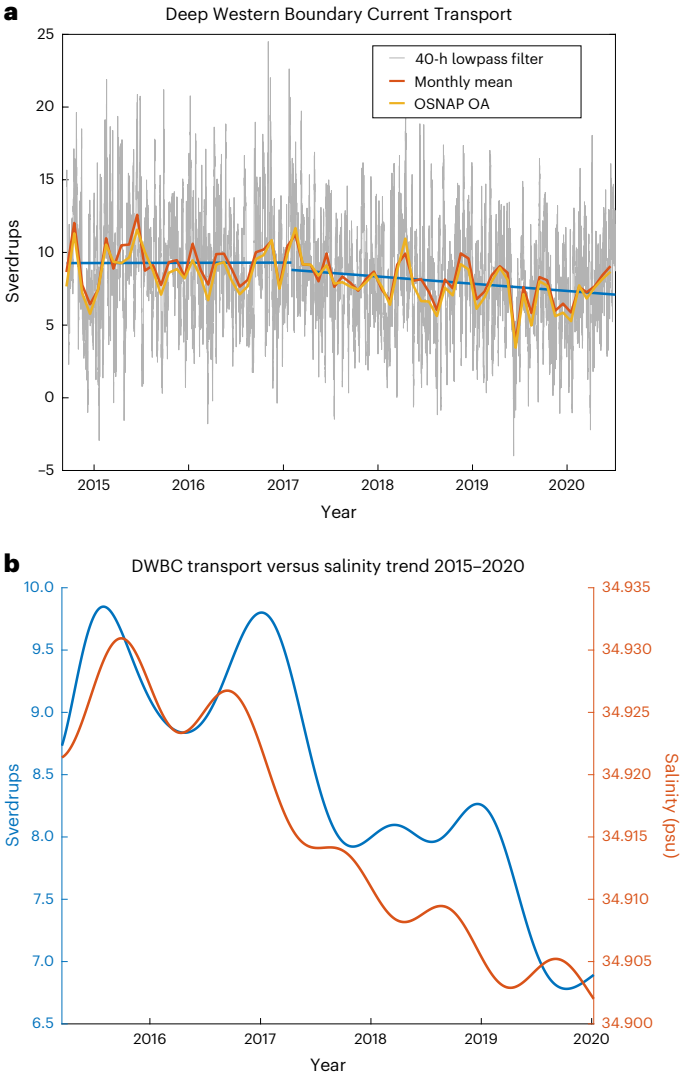

Fig. 2 | Transport and salinity trends of the DWBC. a, A 40-h lowpass-filtered time series of the DWBC transport (grey) overlaid with the monthly mean (red), the monthly mean from the OSNAP objective analysis (OSNAP OA, yellow) and the linear trends for August 2014 to January 2016 and February 2016 to July 2020 (blue). **b**, A 1-year lowpass-filtered time series of DWBC transport (blue) and mean salinity within the DWBC layer (red).

the same mooring locations from September 2014 to July 2016. They found a mean transport of 10.8 ± 4.9 Sv (mean ± standard deviation) for water $\sigma_\theta > 27.8$ kg m^{-3}. In this study, we use the same 2014–2016 mooring data as Hopkins et al.[25] extended by four more years to 2020, although this study uses a different interpolation technique to estimate transport (Methods).

Continuous long-term observations of the DWBC will help to determine how the AMOC may be changing in a warming climate, including concerns about a possible weakening in the twenty-first century and potential collapse on longer time scales[26,27]. This analysis provides results from nearly 6 years (70 months, but henceforth referred to as 6 years) of continuous transport observations of the DWBC from OSNAP. This study reveals that the DWBC has experienced a notable inter-annual weakening since the start of 2017 despite a steady AMOC. Furthermore, this study finds that the varying isopycnal of the monthly maximum in the overturning streamfunction used to define the AMOC has been progressively lightening and that the AMOC would be experiencing a statistically significant transport decrease if it were evaluated using a constant isopycnal like the DWBC transport is evaluated here.

The mean state of the DWBC

Six years of continuous observations of the DWBC reveal a mean transport of 8.5 ± 0.8 Sv (mean ± standard error; positive is southwards) with a standard deviation of 3.9 Sv (Fig. 2a). This compares well with the DWBC mean transport from the OSNAP objective analysis[28,29] of 8.3 Sv, particularly because we would expect a slightly lower transport value near the sea floor due to the more course spatial gridding of the OSNAP objective analysis. However, our transport estimate is more than 2 Sv less than the 2-year DWBC mean from Hopkins et al.[25] of 10.8 Sv. If we compare our transport over the same period as Hopkins et al.[25], our mean transport is closer (9.3 Sv), although still 1.5 Sv lower. The OSNAP objective analysis for a similar time frame yields a mean transport of 8.8 Sv. While these differences may be due to the different methods used to calculate transport across the mooring section, we have confidence in our transport calculation owing to the multiple methods used to account for bottom triangles between moorings (Methods) and our expectedly slightly higher transport than the OSNAP objective analysis. We can further analyse the DWBC transport by separating it into its two primary water masses: Northeast Atlantic deep water (NEADW; traditionally defined as $27.88 > \sigma_\theta > 27.8$ kg m^{-3} (ref. 16)) and Denmark Strait overflow water (DSOW; $\sigma_\theta > 27.88$ kg m^{-3}). Our 6-year analysis of transports of DSOW yields a mean transport of 2.8 ± 0.4 Sv with a standard deviation of 1.5 Sv. The mean from the OSNAP objective analysis is 2.4 Sv. For NEADW, our 6-year mean transport is 5.7 ± 0.7 Sv with a standard deviation of 3.6 Sv. The mean from the OSNAP objective analysis is 5.8 Sv.

The mean velocity cross-section reveals that the DWBC consists of several separate velocity cores (Fig. 3a). Much of the upper NEADW portion of the DWBC appears to be transported by a deep extension of the East Greenland–Irminger Current[30,31] between 1,400 and 1,800 m and moorings CF5 and CF7. The deeper portions of the DWBC appear as two boundary-intensified flows extending along the bottom from mooring M1 down towards M2 and near mooring M3. From these locations, velocities decrease eastwards until the near-bottom southward velocities are offset by northward velocities in the shallower portion of the DWBC and the depth-integrated mean transport (m^2 s^{-1}) for the DWBC ($\sigma_\theta > 27.8$ kg m^{-3}) reaches zero near mooring FLMB.

https://doi.org/10.1038/s41561-024-01555-6

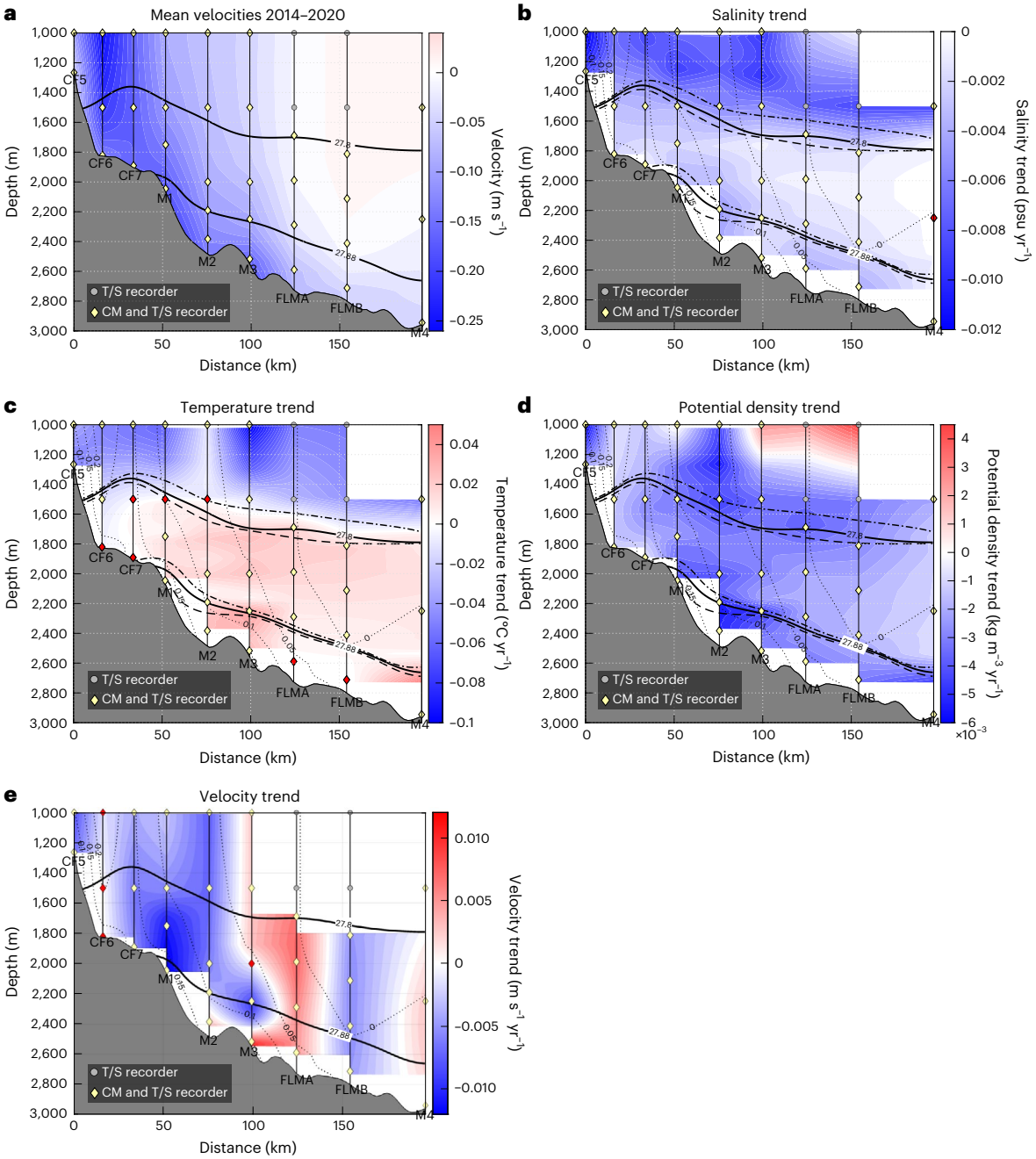

Fig. 3 | Cross-sections of mean velocity and property trends of the DWBC. **a**, Mean velocity cross-section between moorings CF5 and M4 below 1,000 m. **b**, Salinity trend (psu yr^{-1}). **c**, Temperature trend (°C yr^{-1}). **d**, Potential density trend (kg m^{-3} yr^{-1}). **e**, Velocity trend (m s^{-1} yr^{-1}) across the same section. Moorings are labelled with instrument locations from the 2018–2020 deployment, and thick black contours denote the mean σ_θ = 27.8 kg m^{-3} and σ_θ = 27.88 kg m^{-3} isopycnals. In **b**–**d**, the mean σ_θ = 27.8 kg m^{-3} and σ_θ = 27.88 kg m^{-3} isopycnals from the first year of data (dotted–dashed line) and last year of data (dashed line) are presented to illustrate the deepening isopycnals. In **b**–**e**, the thin black dotted velocity contours from **a** are presented in 0.05 m s^{-1} increments. Negative velocity trends in **e** indicate slowing southward velocities (blue). Red instruments have trends that are not statistically significant ($P \geq 0.05$) in **b**–**e**. CM, current meter; T/S recorder, temperature/salinity recorder.

Freshening's role in the decreasing transport of the DWBC

The DWBC 6-year transport (Fig. 2a) reveals that a −0.44 ± 0.02 Sv yr^{-1} decrease has occurred during the observation period (2014–2020). Separating this into the two primary water masses transported by the DWBC, the DSOW transport has decreased at a rate of −0.20 ± 0.01 Sv yr^{-1} while the NEADW transport accounts for the remaining −0.23 ± 0.02 Sv yr^{-1} (Supplementary Table 1). This has resulted in a 26% decrease in the DWBC transport, a 21% decrease in NEADW transport and a 32% decrease in DSOW transport. Some of the DWBC transport decrease appears to be due to an unprecedented freshening signal that has recently been propagating around the upper subpolar gyre[32–35] and entraining into the deep ocean[36–38]. The arrival of this fresh anomaly at the DWBC mooring section in 2017 is synchronous with the start of the DWBC's decreasing transport (Fig. 2b), and further analysis shows that the entirety of the DWBC transport decrease has occurred since 2017. From September 2014 to January 2017, the DWBC has virtually no trend (+0.01 ± 0.10 Sv yr^{-1}), but from

https://doi.org/10.1038/s41561-024-01555-6

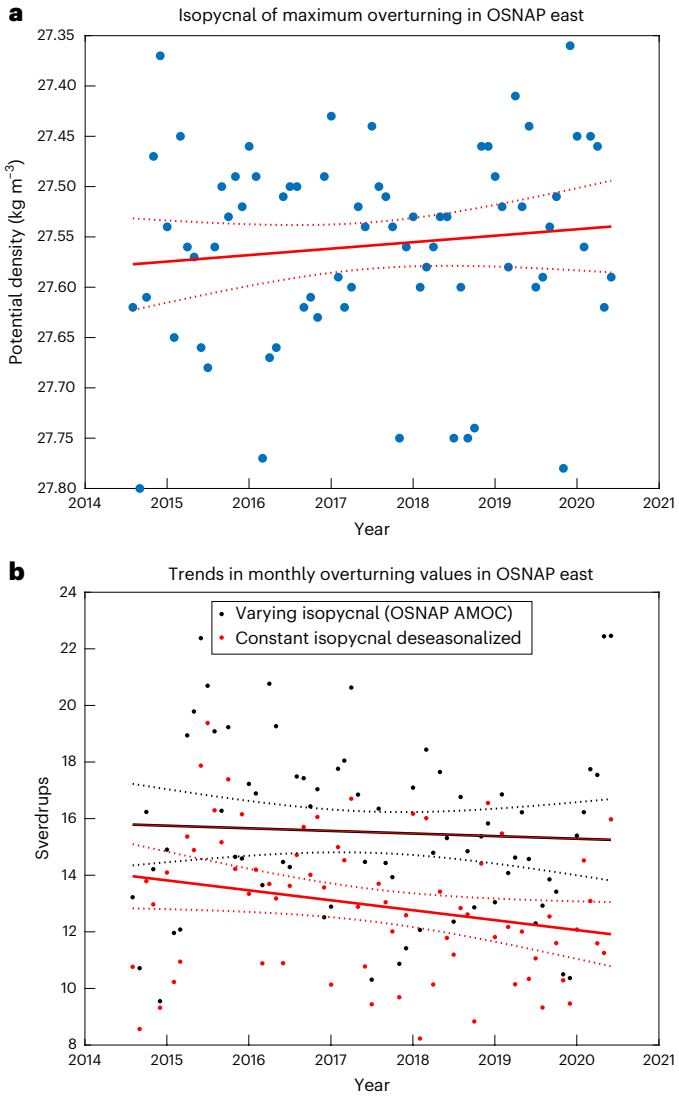

Fig. 4 | Analysis of the isopycnal used to calculate the AMOC. a, A scatterplot of the monthly isopycnal of the overturning streamfunction maximum overlaid with the linear trend and 95% confidence interval. **b**, Scatterplots of AMOC transports using a varying isopycnal (black) and a constant mean isopycnal of $\sigma_\theta = 27.56$ kg m^{-3} with seasonality removed (red). Both scatterplots are overlaid with their respective linear regressions with 95% confidence intervals.

February 2017 onwards the trend is −0.50 ± 0.05 Sv yr^{-1}. Over the same two periods (2014–2017 and 2017–2020), DSOW transport increased by 0.20 ± 0.03 Sv yr^{-1} before decreasing by −0.29 ± 0.02 Sv yr^{-1}, while NEADW saw a relatively steady decline over both time periods (−0.18 ± 0.07 Sv yr^{-1} and −0.21 ± 0.04 Sv yr^{-1}, respectively). Continued freshening after 2017 corresponds with the continued transport decrease of the DWBC. This results in a 0.81 correlation for the 1-year lowpass-filtered time series of the mean salinity and transport. A 1-year lowpass filter was used to evaluate inter-annual changes, such as the freshening signal, by removing variability on seasonal time scales and shorter.

The freshening signal is pervasive throughout the entire water column as every location in the mooring cross-section has freshened since the first year of OSNAP (Fig. 3b). While the DWBC has not freshened as dramatically as shallower waters, the DWBC has also warmed since the start of OSNAP (Fig. 3c) and contributes to decreasing densities in the DWBC (Fig. 3d). This warming is mainly driven by the downward isopycnal displacement within the DWBC layer related to the freshening event[37]. The deep isopycnals sink as the DWBC waters become lighter and fresher, shrinking the DWBC layer and warming the deep Irminger Sea. Indeed, in some instances, the isopycnal used to define the top of the DWBC ($\sigma_\theta = 27.8$ kg m^{-3}) has deepened by more than 160 m during the OSNAP observation period (Fig. 3b–d). Overall, the cross-sectional areas of the full DWBC layer (NEADW plus DSOW) and the DSOW layer alone across our mooring section have decreased by 15.6 ± 0.2% and 29.6 ± 0.3%, respectively (Supplementary Fig. 1). While these decreasing cross-sectional areas are the primary reason for the decreasing transports (56% for DWBC and 75% for DSOW), the remaining decreases (44% and 25%, respectively) are due to the mean velocities within each water mass decreasing by 12.4 ± 1.5% in the DWBC and 10.0 ± 1.4% in DSOW (Methods and Supplementary Fig. 2). This velocity reduction is seen throughout the entire water column across most of the mooring section from CF5 to M3, with the greatest velocity reduction near mooring M1 (Fig. 3e and Supplementary Fig. 3). To further consider this velocity decrease, we calculated the time-varying transport of the DWBC using the 6-year mean depth of the isopycnal ($\sigma_\theta = 27.8$ kg m^{-3}; Fig. 3) to evaluate velocities within a static layer and found a 14.6 ± 1.4% decrease in the velocities in the layer. A notable feature in the velocity trend (Fig. 3e) is the offshore alternating velocity reversals at moorings FLMA, FLMB and M4. We believe this feature is mostly due to high variability from mesoscale activity in the basin interior[39]. Interestingly, most of the thinning of the DWBC occurs before the start of the transport reduction in 2017 (Supplementary Fig. 1a) because it was offset by velocity increases across the section (Supplementary Fig. 2a). The effect of the thinning layer only began to reduce transports once the velocities began to decrease starting in 2017.

Reconciling a decreasing DWBC with a stable AMOC

While our analysis and the OSNAP objective analysis agree that the DWBC east of Greenland has seen a notable decrease in transport, the OSNAP-calculated AMOC has remained relatively stable despite the DWBC being the primary constituent of the lower limb of the AMOC[29,40]. Much of the reason for this is due to the different methods used in each calculation. Our study calculates the DWBC using the traditional method of estimating the transport of all water denser than a constant isopycnal ($\sigma_\theta = 27.8$ kg m^{-3}). The AMOC, however, is calculated using a time-varying isopycnal based on the monthly maximum in the transport overturning streamfunction in density space[28]. In 6 years of OSNAP data, this isopycnal has varied widely for OSNAP East (Greenland–Scotland OSNAP section), from 27.36 to 27.8 kg m^{-3} (Fig. 4a), and has a statistically insignificant transport decrease of −0.09 ± 0.21 Sv yr^{-1}. If instead a constant isopycnal is used—the mean isopycnal of the monthly OSNAP overturning streamfunction maxima ($\sigma_\theta = 27.56$ kg m^{-3})—and seasonality is removed[29], we find the AMOC has decreased over the 6-year record at a rate of −0.35 ± 0.17 Sv yr^{-1}, which is statistically significant at a 95% confidence threshold with a P value of 0.04 (Fig. 4b). Most of this change is due to the constant isopycnal (69%), although removing seasonality also plays an important role (31%). The method of calculating the AMOC using a constant isopycnal has also recently revealed a greater contribution to the AMOC from the Labrador Basin[41]. One trend that has emerged from the method used by OSNAP to evaluate the AMOC is a lightening of the isopycnal of maximum overturning streamfunction during the 6-year record by 0.006 ± 0.007 kg m^{-3} yr^{-1} (Fig. 4a), although this trend only has a P value of 0.35.

The lightening of the isopycnal of maximum overturning relates to the decreasing transport of the DWBC in that the entire lower limb of the AMOC is becoming less dense. As the deepest layers thin, lighter water becomes a new component of the upper portion of the lower limb, and as the AMOC evolves in a changing climate, how we define these water masses becomes more critical. In fact, if we use a different definition for NEADW (practical salinity >34.92 and $\sigma_\theta > 27.74$ kg m^{-3} (ref. 42)), we find that the water mass virtually disappears during the

OSNAP record owing to the low-salinity anomaly. Moving forward, new methods for evaluating the AMOC that better resolve the water mass changes that occur within the AMOC should be considered; likewise, the DWBC would be better evaluated using definitions beyond a single isopycnal that give greater consideration to the sources of its water masses, and we hope this Article serves as a catalyst for future investigations into this topic. Further observations in the subpolar region will help determine the new methods and examine the impact of the density changes found in this study on a warming climate.

Online content

Any methods, additional references, Nature Portfolio reporting summaries, source data, extended data, supplementary information, acknowledgements, peer review information; details of author contributions and competing interests; and statements of data and code availability are available at https://doi.org/10.1038/s41561-024-01555-6.

References

1. Buckley, M. W., Lozier, M. S., Desbruyères, D. & Evans, D. G. Buoyancy forcing and the subpolar Atlantic Meridional Overturning Circulation. *Philos. Trans. R. Soc. A* **381**, 20220181 (2023).
2. Johns, W. E., Devana, M., Houk, A. & Zou, S. Moored observations of the Iceland–Scotland overflow plume along the eastern flank of the Reykjanes Ridge. *J. Geophys. Res. Oceans* **126**, e2021JC017524 (2021).
3. Zou, S. J., Lozier, S., Zenk, W., Bower, A. & Johns, W. Observed and modeled pathways of the Iceland Scotland overflow water in the eastern North Atlantic. *Prog. Oceanogr.* **159**, 211–222 (2017).
4. Bower, A. S., Lozier, M. S., Gary, S. F. & Boning, C. W. Interior pathways of the North Atlantic Meridional Overturning Circulation. *Nature* **459**, 243–247 (2009).
5. Bilo, T. C. & Johns, W. E. Interior pathways of Labrador Sea water in the North Atlantic from the Argo perspective. *Geophys. Res. Lett.* **46**, 3340–3348 (2019).
6. McCarthy, G. D. et al. Sustainable observations of the AMOC: methodology and technology. *Rev. Geophys.* **58**, e2019RG000654 (2020).
7. Eldevik, T., Nilsen, J. E. Ø., Iovino, D., Anders Olsson, K., Sandø, A. B. & Drange, H. Observed sources and variability of Nordic seas overflow. *Nat. Geosci.* **2**, 406–410 (2009).
8. Våge, K. et al. The Irminger Gyre: circulation, convection, and interannual variability. *Deep Sea Res. Part I* **58**, 590–614 (2011).
9. Bacon, S. Decadal variability in the outflow from the Nordic seas to the deep Atlantic Ocean. *Nature* **394**, 871–874 (1998).
10. Dickson, R. R. & Brown, J. The production of North Atlantic deep water: sources, rates, and pathways. *J. Geophys. Res.: Oceans* **99**, 12319–12341 (1994).
11. McCartney, M. S. Recirculating components to the deep boundary current of the northern North Atlantic. *Prog. Oceanogr.* **29**, 283–383 (1992).
12. Clarke, R. A. Transport through the Cape Farewell-Femish Cap section. *Rapp. P. V. Reu. Cos. Int. Explor. Mer.* **185**, 120–130 (1984).
13. Lozier, M. S. et al. Overturning in the Subpolar North Atlantic Program: a new international ocean observing system. *Bull. Am. Meteorol. Soc.* **98**, 737–752 (2017).
14. Lozier, M. S. et al. A sea change in our view of overturning in the subpolar North Atlantic'. *Science* https://doi.org/10.1126/science.aau6592 (2019).
15. Lozier, M. S. Overturning in the subpolar North Atlantic: a review. *Philos. Trans. R. Soc. A* **381**, 20220191 (2023).
16. Holliday, N. P., Bacon, S., Allen, J. & McDonagh, E. L. Circulation and transport in the western boundary currents at Cape Farewell, Greenland. *J. Phys. Oceanogr.* **39**, 1854–1870 (2009).
17. Bacon, S. & Saunders, P. M. The Deep Western Boundary Current at Cape Farewell: results from a moored current meter array. *J. Phys. Oceanogr.* **40**, 815–829 (2010).
18. Bacon, S. Circulation and fluxes in the North Atlantic between Greenland and Ireland. *J. Phys. Oceanogr.* **27**, 1420–1435 (1997).
19. Bersch, M. On the circulation of the northeastern North Atlantic. *Deep Sea Res. Part I* **42**, 1583–1607 (1995).
20. Daniault, N. et al. The northern North Atlantic Ocean mean circulation in the early 21st century. *Prog. Oceanogr.* **146**, 142–158 (2016).
21. Holliday, N. P. et al. Subpolar North Atlantic overturning and gyre-scale circulation in the summers of 2014 and 2016. *J. Geophys. Res. Oceans* **123**, 4538–4559 (2018).
22. Lherminier, P. et al. Transports across the 2002 Greenland–Portugal Ovide section and comparison with 1997. *J. Geophys. Res. Oceans* https://doi.org/10.1029/2006JC003716 (2007).
23. Lherminier, P. et al. The Atlantic Meridional Overturning Circulation and the subpolar gyre observed at the A25-OVIDE section in June 2002 and 2004. *Deep Sea Res. Part I* **57**, 1374–1391 (2010).
24. Sarafanov, A. et al. Mean full-depth summer circulation and transports at the northern periphery of the Atlantic Ocean in the 2000s. *J. Geophys. Res. Oceans* https://doi.org/10.1029/2011JC007572 (2012).
25. Hopkins, J. E. et al. Transport variability of the Irminger Sea Deep Western Boundary Current from a mooring array. *J. Geophys. Res. Oceans* **124**, 3246–3278 (2019).
26. Boers, N. Observation-based early-warning signals for a collapse of the Atlantic Meridional Overturning Circulation. *Nat. Clim. Change* **11**, 680–688 (2021).
27. Caesar, L., Rahmstorf, S., Robinson, A., Feulner, G. & Saba, V. Observed fingerprint of a weakening Atlantic Ocean overturning circulation. *Nature* **556**, 191–196 (2018).
28. Li, F., Lozier, M. S. & Johns, W. E. Calculating the meridional volume, heat, and freshwater transports from an observing system in the subpolar North Atlantic: observing system simulation experiment. *J. Atmos. Ocean. Technol.* **34**, 1483–1500 (2017).
29. Fu, Yao et al. Seasonality of the meridional overturning circulation in the subpolar North Atlantic. *Commun. Earth Environ.* **4**, 1–13 (2023).
30. Le Bras, I. A.-A., Straneo, F., Holte, J. & Holliday, N. P. Seasonality of freshwater in the East Greenland current system from 2014 to 2016. *J. Geophys. Res. Oceans* **123**, 8828–8848 (2018).
31. Daniault, N., Mercier, H. & Lherminier, P. The 1992–2009 transport variability of the East Greenland–Irminger Current at 60°N. *Geophys. Res. Lett.* https://doi.org/10.1029/2011GL046863 (2011).
32. Holliday, N. P. et al. Ocean circulation causes the largest freshening event for 120 years in eastern subpolar North Atlantic. *Nat. Commun.* **11**, 585 (2020).
33. Fox, A. D. et al. Exceptional freshening and cooling in the eastern subpolar North Atlantic caused by reduced Labrador Sea surface heat loss. *Ocean Sci.* **18**, 1507–1533 (2022).
34. Zhang, J. et al. Labrador Sea freshening linked to Beaufort Gyre freshwater release. *Nat. Commun.* **12**, 1229 (2021).
35. Biló, T. C., Straneo, F., Holte, J. & Le Bras, I. A. Arrival of new great salinity anomaly weakens convection in the Irminger Sea. *Geophys. Res. Lett.* **49**, e2022GL098857 (2022).
36. Devana, M. S., Johns, W. E., Houk, A. & Zou, S. Rapid freshening of Iceland Scotland overflow water driven by entrainment of a major upper ocean salinity anomaly. *Geophys. Res. Lett.* **48**, e2021GL094396 (2021).
37. Desbruyères, D. G. et al. Warming-to-cooling reversal of overflow-derived water masses in the Irminger Sea during 2002–2021. *Geophys. Res. Lett.* **49**, e2022GL098057 (2022).

38. Chafik, L. & Holliday, N. P. Rapid communication of upper-ocean salinity anomaly to deep waters of the Iceland Basin indicates an AMOC short-cut. *Geophys. Res. Lett.* **49**, e2021GL097570 (2022).
39. Fischer, J. et al. Intra-seasonal variability of the DWBC in the western subpolar North Atlantic. *Prog. Oceanogr.* **132**, 233–249 (2015).
40. Fu, Y., Li, F., Karstensen, J. & Wang, C. A stable Atlantic Meridional Overturning Circulation in a changing North Atlantic Ocean since the 1990s. *Sci. Adv.* **6**, eabc7836 (2020).
41. Le Bras, I. A. Labrador Sea water spreading and the Atlantic Meridional Overturning Circulation. *Philos. Trans. R. Soc. A* **381**, 20220189 (2023).
42. Pacini, A. et al. Mean conditions and seasonality of the West Greenland boundary current system near Cape Farewell. *J. Phys. Oceanogr.* **50**, 2849–2871 (2020).
43. Koman, G., Johns, W. E. & Houk, A. Transport and evolution of the East Reykjanes Ridge current. *J. Geophys. Res.* **125**, e2020JC016377 (2020).

Methods

OSNAP has maintained mooring observations of transport, heat flux and freshwater flux across the entire subpolar North Atlantic from Labrador to Scotland since 2014. To evaluate the DWBC, this study uses seven OSNAP moorings (CF5, CF6, CF7, M1, M2, M3 and M4) and two moorings from the National Science Foundation Ocean Observatories Initiative's Global Irminger Sea Array (FLMA and FLMB) located across the continental slope east of Greenland near Cape Farewell. These moorings provide continuous observations using temperature–salinity sensors, current meters and downward-facing ADCPs near the bottom (for the first four years of deployment; Fig. 3a). The observations used in this study extend for nearly 70 months, from 16 September 2014 to 8 July 2020. For simplicity, this study refers to this time frame as '6 years'. More information about OSNAP moorings and instrumentation can be found at www.o-snap.org. More information about the National Science Foundation Ocean Observatories Initiative's Global Irminger Sea Array can be found at https://oceanobservatories.org/array/global-irminger-sea-array.

Temperature, salinity and velocity data are collected at 30 min intervals, then a 40 h lowpass filter is applied. The data are then interpolated into 6 h intervals in time. Shape-preserving (pchip) splines are used to grid the data into 2-m-depth intervals, and linear interpolation is used to grid the data in ~2 km intervals along the mooring line. Missing instrument data are filled using the linear relationship of non-missing observations from adjacent depths. When necessary, velocity data are extended as a constant to shallower depths at moorings FLMA, FLMB and M4 for transport calculations. Velocity vectors are rotated to be normal to the mooring line as calculated from the two outermost moorings used in this study (CF5 and M4). This results in a vector rotation angle of 190.1°. Transports in the full DWBC layer are calculated by integrating velocities (in x and z) that have $\sigma_\theta > 27.8$ kg m^{-3}. This method is different from the one used by Hopkins et al.[25] as they used variance ellipses of the data that incorporate decorrelation length scales between instruments (in both the horizontal and vertical) in an iterative objective analysis to interpolate temperature, salinity and velocity measurements from fixed sensors. Transports in the two constituent layers of the DWBC, NEADW and DSOW are calculated by integrating velocities (in x and z) that have 27.88 kg m^{-3} > σ_θ > 27.8 kg m^{-3} and σ_θ > 27.88 kg m^{-3}, respectively. DWBC and DSOW cross-sectional areas are calculated using the same method as the transport calculation, but all velocities within the evaluation regions (σ_θ > 27.8 kg m^{-3} and σ_θ > 27.88 kg m^{-3}, respectively) are changed to 1 and all velocities outside the region are set to zero.

Due to the bottom-intensified nature of the DWBC, properly estimating transport from fixed instruments over a sloping bottom in the unsampled bottom triangles between moorings is of utmost importance. Therefore, this study calculated the DWBC and DSOW transports using four different methods to estimate the bottom triangles and then used the mean of the four methods to determine our final transport calculation. Three of the methods extend the velocity measured at the deepest instrument of the shallower mooring downward (below the sea floor) to a depth that matches the deepest instrument on the deeper mooring, followed by linear interpolation between the moorings. The three methods used to extend the velocity measured at the deepest instrument on the shallower mooring were (1) extending the deepest velocity of the shallower mooring as a constant, (2) using the velocity shear between the deepest instruments of the shallower and deeper mooring (as used in ref. 2) and (3) applying the velocity shear at the bottom of the deeper mooring to the deepest velocity of the shallower mooring. The fourth method calculated transport using height above bottom as the vertical coordinate, which effectively shifts the moorings as if they were along a flat bottom (and shifts the unsampled triangles to the top of the water column where we are not calculating transports in this study). These four methods yielded mean DWBC transport values of 8.3–8.7 Sv, which resulted in a mean of 8.5 Sv, and we included 0.2 Sv of error in the standard error to account for this range. We chose to use the mean since we cannot determine which estimate is best among four viable options. A bottom boundary layer that linearly decreases velocities to zero in the bottom 30 m is also applied to all transport calculations.

For simplicity, the text presents velocity decreases as a percentage, although the linear trend of the DWBC is $-1.174 \times 10^{-3} \pm 1.039 \times 10^{-3}$ m s^{-1} yr^{-1} (trend ± standard error). For the DSOW transport, the trend is $-1.114 \times 10^{-3} \pm 1.261 \times 10^{-3}$ m s^{-1} yr^{-1}. In these estimates, we incorporate the integral time scales of the data (6.7 days for DWBC and 7.2 days for DSOW) to estimate degrees of freedom and standard errors. The DWBC, NEADW and DSOW transport trends (Supplementary Table 1) were calculated in a similar manner.

The OSNAP objective analysis product, which is used in this Article to compare DWBC results and analyse changes to the AMOC, is a monthly integrated analysis of all OSNAP observations across the trans-basin array[13,28]. In addition to OSNAP observations, the objective analysis incorporates other observations, including Argo floats and satellite altimetry, and applies a mass balance to determine fluxes of mass, heat and freshwater across the subpolar gyre. Details of this method can be found in Li et al.[28]. For this Article, we use OSNAP objective analysis data for OSNAP east, which is the region between Greenland and Scotland. When the OSNAP objective analysis is compared with Hopkins et al.[25], the period of October 2015 to June 2017 is used.

Data availability

The 2014–2020 OSNAP MOC and gridded velocity products are available in SMARTech Repository (https://doi.org/10.35090/gatech/70342) and are freely available at www.o-snap.org.

Code availability

Code will be made available upon request to the corresponding author.

Acknowledgements

This work was supported with funding from the US National Science Foundation through grant numbers OCE 1756363 (G.K., A.S.B. and H.H.F.) and OCE 1948505 (G.K., A.S.B. and H.H.F.) to the Woods Hole Oceanographic Institution. N.P.H. was supported by UK Natural Environment Research Council (NERC) grants CLASS (NE/R015953/1), UK-OSNAP (NE/K010875/2) and UK OSNAP Decade (NE/T00858X/1). Y.F. acknowledges funding from the Physical Oceanography Program of the US National Science Foundation (OCE-1948335). T.C.B. gratefully acknowledges the funding from the National Science Foundation under grants OCE 1258823 and OCE 1756272; NOAA's Global Ocean Monitoring and Observing programme (FundRef number 100007298); NOAA's Climate Program Office, Climate Observations and Monitoring, and Climate Variability and Predictability programmes under NOFO NOAA-OAR-CPO-2021-2006389 with additional NOAA Atlantic Oceanographic and Meteorological Laboratory support. This research was carried out in part under the auspices of the Cooperative Institute for Marine and Atmospheric Studies, a cooperative institute of the University of Miami and the National Oceanic and Atmospheric Administration (NOAA), cooperative agreement NA 20OAR4320472. OSNAP data were collected and made freely available by the OSNAP project and all the national programmes that contribute to it (www.o-snap.org).

Author contributions

A.S.B. and N.P.H. acquired financial support for the projects leading to this publication. G.K., A.S.B., N.P.H., H.H.F. and T.C.B. were responsible for data collection, processing and quality control. G.K. completed data analysis and calculations. Y.F. synthesized all OSNAP programme data into OSNAP objective analysis. G.K. wrote the initial draft and

created visualizations. G.K., A.S.B., N.P.H., H.H.F., Y.F. and T.C.B. reviewed and edited the manuscript.

Competing interests
The authors declare no competing interests.

Additional information
Supplementary information The online version contains supplementary material available at https://doi.org/10.1038/s41561-024-01555-6.

Correspondence and requests for materials should be addressed to G. Koman.

Peer review information *Nature Geoscience* thanks M. Dolores Pérez-Hernández and the other, anonymous, reviewer(s) for their contribution to the peer review of this work. Primary Handling Editor: James Super, in collaboration with the *Nature Geoscience* team.